SCIEPublish

*Article*

# Influence of Soil Damping and Aerodynamic Damping on the Dynamic Response of Monopile Wind Turbines under Earthquake and Wind Loads

**Piguang Wang [1,2], Yang Bai [2], Renqiang Xi [3,*], Yang Qu [2] and Xiuli Du [2]**

[1] Chongqing Research Institute, Beijing University of Technology, Chongqing 401152, China; wangpiguang1985@126.com (P.W.)

[2] The Key Laboratory of Urban Security and Disaster Engineering of Ministry of Education, Beijing University of Technology, Beijing 100124, China; yangbai183@163.com (Y.B.); yangqu@bjut.edu.cn (Y.Q.); duxiuli@bjut.edu.cn (X.D.)

[3] School of Mechanical Engineering and Rail Transit, Changzhou University, Changzhou 213164, China

* Corresponding author. E-mail: xirenqiang@cczu.edu.cn (R.X.)

Received: 7 January 2025; Accepted: 10 March 2025; Available online: 12 March 2025

**ABSTRACT:** Vibration damping is essential for predicting the responses of wind turbines, and contributions mainly come from structural, soil, and aerodynamic damping. In engineering design, it is difficult to precisely account for the individual contributions of each damping source. As a result, a simplified approach is commonly used, where a total damping factor is applied that combines the effects of structural, soil, aerodynamic, and other damping sources. However, the accuracy of this simplified approach in predicting the dynamic response of turbines has not been thoroughly evaluated. This study primarily focuses on the applicability of vibration-damping simplification methods, particularly in analyzing the dynamic response of turbines under earthquake and wind loads.

**Keywords:** Wind turbine; Soil damping; Aerodynamic damping; Dynamic response



## 1. Introduction

The wind energy industry has expanded rapidly worldwide due to environmental concerns [1]. Wind turbines (WT) are typically tall, slender structures and natural frequencies close to environmental loads. As a result, their dynamic response and fatigue need to be considered during the design process. Many WTs are also installed in high seismic risk regions, such as the western United States, southern Europe, New Zealand, and the eastern coast of China [2]. Therefore, earthquake effects must be incorporated into wind turbine designs. In addition, vibration damping plays a crucial role in reducing dynamic response amplitude, making it an essential factor in predicting the dynamic response of WTs. A simplified damping model, incorporating damping factors from structural, soil, aerodynamic, and other sources, is widely used to analyze the fatigue life of WTs [3]. Shirzadeh et al. [4], through the experiments in the Belgian North Sea and corresponding numerical simulations, found that using the sum of individual damping as the total damping of the structure has a little error with the experimentally measured damping ratio of the structure. In the subsequent studies, Cheng et al. [5] calculated the response of the WTs under wind and wave loads, ignoring the pile-soil interaction and assuming a total damping ratio of 2.5. For the study of the dynamic characteristics of the WTs under parked, Wang et al. [6] simplified the structural, soil, and other damping to a 5% Rayleigh damping. Ali et al. [7] simplified the structural, soil, aerodynamic, and other sources of damping to a total 3% damping ratio in their study of the fragility of OWTs under wind and seismic loads. However, incorrect consideration of vibration damping can significantly affect the prediction of dynamic response, leading to either overly conservative or unsafe designs. Therefore, it is essential to evaluate the precision of the simplified damping model when predicting the wind turbine's dynamic response under earthquake and environmental loads.

Aerodynamic damping is caused by the aeroelastic effect of WTs and can be significantly higher than structural damping [4]. It primarily depends on factors such as rotor speed, airfoil shape and size, and incoming wind conditions.

https://doi.org/10.70322/mer.2025.10003

For wind turbines with different capacities and operating conditions, using the same aerodynamic damping values may not be appropriate. Additionally, aerodynamic damping is greater in the along-wind direction compared to other directions. Chen et al. [3] suggested a range of 5% to 7% for aerodynamic damping. Take an OWT under operation as an example, the aerodynamic damping in the along-wind direction can be 5 to 10 times greater than in the across-wind direction [8]. Therefore, it is crucial to consider aerodynamic damping in numerical studies thoroughly. The dynamic behavior of a WT during operation is often influenced by aerodynamic coupling effects. Feyzollahzadeh et al. [9] studied the dynamic characteristics of FOWTs, while Rendon and Manuel [10] highlighted that the tower's dynamic response varies with changes in wind speed and wave height. The decoupling method is currently the primary approach used to calculate aerodynamic damping in WTs. Several models for aerodynamic damping in both onshore and offshore wind turbines were established by Garrad et al. [11]. Considering the effect of wind speed, Chen and Duffour [3], and Chen et al. [12], introduced a semi-analytic approach that incorporates aerodynamic damping ratios in the fore-aft and side-to-side using element momentum theory. However, their models do not account for the damping coupling between motions in the FA and SS directions.

Soil damping plays a crucial role in predicting the dynamic response of WTs, particularly for parked wind turbines. It consists of hysteretic material damping and radiation damping, which arises from diffracted waves spreading away from the pile [13,14]. Radiation damping is influenced by factors such as the frequency of external excitation, shear wave velocity of the soil, and pile diameter [15,16]. Recent studies have explored the soil damping of wind turbines, with measurements from OWTs indicating values between 0.25% and 1.5% [17]. Shirzadeh et al. [4] used the PolyMAX to estimate the soil damping contribution for the first mode of OWT, finding it to be 0.25%. Similarly, Tarp-Johansen et al. [18], using finite element analysis, estimated the soil damping for a monopile OWT, with values ranging from 0.56% to 0.80%. In subsequent studies, Carswell et al. [13] observed that soil damping values varied between 0.17% and 0.28%, reducing the dynamic response of monopile OWTs by 7–9%. Damgaard et al. [19] introduced hysteretic springs to model the SSI, determining that the soil damping contribution ranged from 0.8% to 1.3%. In a different study, Jiang et al. [20] proposed a method to calculate soil damping in offshore wind turbines (OWTs) with wide-shallow bucket foundations, taking into account soil hysteresis properties. Their findings indicated that soil damping increases as the compression modulus increases and the plasticity index decreases, highlighting the influence of soil characteristics on the damping behavior in these types of foundations.

While vibration damping in both marine and terrestrial wind turbines has been thoroughly studied, the influence of soil and aerodynamic damping on the dynamic behavior of WTs subjected to earthquake and environmental loads remains poorly understood. Current designs often combine soil and aerodynamic damping into aggregate structural damping. However, the precision of simplified damping approaches for predicting the dynamic response of WTs has not been researched. Therefore, this study focuses on the effects of soil and aerodynamic damping on the dynamic characteristics of WTs subjected to earthquake and wind loads, as well as evaluates the accuracy of the simplified damping approaches commonly used in current designs.

## 2. Descriptions of the Model and Load Cases

A typical 5MW-OWT is illustrated in Figure 1. The details of the structure-soil interaction, the finite element equations governing the OWT, the aerodynamic forces, and the simplified damping model are provided herein.

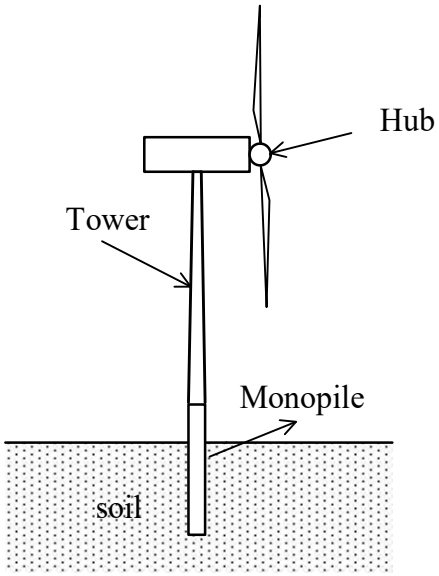


**Figure 1.** A monopile OWT system in the soil.

### *2.1. Pile-Soil Interaction*

According to the authors' previous studies [15], the resistance of the soil can be represented as

$$P_u(z) = \sum_{m=1}^{\infty} F_m z_m \tag{1}$$

$$F_m = S_u u_m \tag{2}$$

$$S_u = \pi G r_0^2 \frac{[2\,K_1(r_0) + r_0\,K_0(r_0)]\,K_1(r_1) + [2\,K_1(r_1) + r_1\,K_0(r_1)]\,K_1(r_0)}{r_1\,K_0(r_1)\,K_1(r_0) + r_0\,K_1(r_1)\,K_0(r_0) + r_0 r_1\,K_0(r_1)\,K_0(r_0)} \tag{3}$$

$$u_m = \frac{2}{h}\int_0^h u z_m dz \tag{4}$$

where $z_m = sin\,\lambda_m z$ ; $\lambda_m = (2m-1)\pi/2h$; $r_1 = r_0/\eta$; $\eta = \sqrt{2(1-\upsilon_s)/(1-2\upsilon_s)}$; $r_0 = \lambda_m a\sqrt{1-\omega_0^2}$; $\omega_0 = \frac{\omega}{\lambda_m v_s}$; $K_1(\cdot)$, $G_0$, $\beta$, $\rho_s$, $\upsilon_s$ and $v_s$ can refer to [15].

Further, the discrete horizontal resistances vector $\boldsymbol{P_u}$ is obtained as

$$\boldsymbol{P}_u = \boldsymbol{S}_u^{\infty}\boldsymbol{u} \tag{5}$$

$$\boldsymbol{S}_u^{\infty} = \boldsymbol{W}\left[\frac{2}{h}\sum_{m=1}^{\infty} S_u\,\boldsymbol{\Phi}_m\boldsymbol{\Phi}_m^T\right]\boldsymbol{W} \tag{6}$$

$$\boldsymbol{W} = \int_0^h \boldsymbol{N}^T\boldsymbol{N}dz \tag{7}$$

where $\boldsymbol{N}$ and $\boldsymbol{\Phi}_m$ can refer to [15].

The displacement of soil in the free field can be calculated ed by [21]:

$$U_f = U_g\,cos\,k\,z + U_g\,tan\,k\,h\,sin\,k\,z - U_g \tag{8}$$

where $k = \omega/v_s$, $\omega$ is the frequency of the earthquake, $U_g = \int_{-\infty}^{\infty} u_g e^{-i\omega t}\,dt$, and $u_g$ is the displacement of the earthquake.

Soil damping gradually increases as the structure transitions from the elastic stage to the nonlinear stage. However, in order to highlight the impact of soil damping on the structure, this study mainly focuses on the case of small strain in the soil when the structure is in the elastic stage.

A set of 22 far-field records from the US FEMA P695 [22] specification is selected in this study. The acceleration response spectra for each time history of this far-field set are presented in Figure 2.

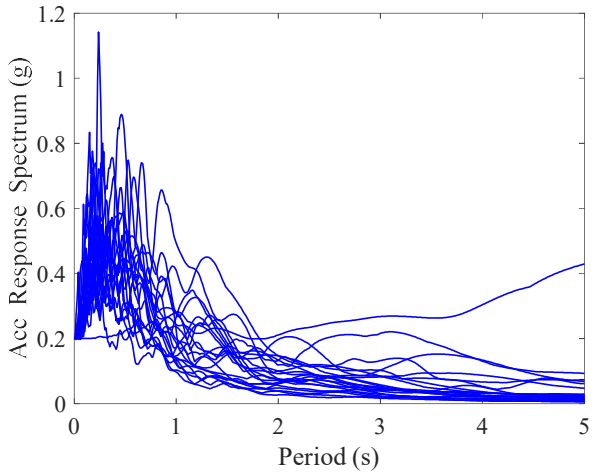


**Figure 2.** The acceleration response spectral of selected records.

### *2.2. Finite Element Equation*

The equation of the SSI of OWT can be expressed as

$$\begin{bmatrix} \boldsymbol{S}_I & \boldsymbol{S}_{IB} \\ \boldsymbol{S}_{BI} & \boldsymbol{S}_B + \boldsymbol{S}_u^{\infty} \end{bmatrix} \begin{Bmatrix} \boldsymbol{U}_I \\ \boldsymbol{U}_B \end{Bmatrix} = \begin{Bmatrix} \boldsymbol{F}_I \\ \boldsymbol{F}_B \end{Bmatrix} \tag{9}$$

$$\begin{bmatrix} \boldsymbol{S}_I & \boldsymbol{S}_{IB} \\ \boldsymbol{S}_{BI} & \boldsymbol{S}_B \end{bmatrix} = -\omega^2 \begin{bmatrix} \boldsymbol{M}_I & 0 \\ 0 & \boldsymbol{M}_B \end{bmatrix} + i\omega \begin{bmatrix} \boldsymbol{C}_I & \boldsymbol{C}_{IB} \\ \boldsymbol{C}_{BI} & \boldsymbol{C}_B \end{bmatrix} + \begin{bmatrix} \boldsymbol{K}_I & \boldsymbol{K}_{IB} \\ \boldsymbol{K}_{BI} & \boldsymbol{K}_B \end{bmatrix} \tag{10}$$

where *B* and *I* denote the pile embedded in soil and in a vacuum, respectively; $\boldsymbol{M}$, $\boldsymbol{K}$, and $\boldsymbol{C}$ are the mass, stiffness, and damping matrices, respectively; $\boldsymbol{U}$ is the flexible displacement vector; $\boldsymbol{F}$ is the discrete force vector acting on the pile and OWT.

The element mass ($\boldsymbol{M_e}$) and stiffness matrices ($\boldsymbol{K_e}$) of the OWT can be expressed as

$$\boldsymbol{M_e} = m_e \begin{bmatrix} \frac{1}{2} & 0 & 0 & 0 \\ 0 & \frac{l^2}{78} & 0 & 0 \\ 0 & 0 & \frac{1}{2} & 0 \\ 0 & 0 & 0 & \frac{l^2}{78} \end{bmatrix} \tag{11}$$

$$\boldsymbol{K_e} = \frac{EI_e}{l^3} \begin{bmatrix} 12 & 6l & -12 & 6l \\ 6l & 4l^2 & -6l & 2l^2 \\ -12 & -6l & 12 & -6l \\ 6l & 2l^2 & -6l & 4l^2 \end{bmatrix} \tag{12}$$

where $E$ is the elasticity modulus, $l$ is the length of the element; $m_e$ is the unit mass of the element; and $I_e$ is the unit moment of inertia.

The tower is represented as a series of segments. The paraments of each segment are given by the expressions provided by Wang et al. [23]. These parameters describe the structural properties of each segment, accounting for variations in geometry and material distribution along the height of the tapered tower.

$$EI_i = \frac{1}{l_i} \int_{z_{i+1}}^{z_i} EI(z)\, dz \tag{13}$$

$$\rho A_i = \frac{1}{l_i}\int_{z_{i+1}}^{z_i} \rho A(z)\, dz \tag{14}$$

where $\rho$ is density, $I(z)$ is inertia moment, $A(z)$ and $l_i$ are the area and length of each segment, respectively.

Then, in the time domain, the response of the OWT can be calculated through the inverse Fourier transform:

$$u = \frac{1}{2\pi}\int_{-\infty}^{\infty} Ue^{i\omega t}\, d\omega \tag{15}$$

### *2.3. Aerodynamic Forces*

The wind acts on the flexible blades of wind turbines; a phenomenon termed the aeroelastic effect. In the frequency domain analysis of a WT's dynamic response, the aerodynamic load on the rotor is split into the load on the undeformed structure and the damping forces. The aerodynamic load acting on the undeformed structure is assumed to act at the center of the top section of the tower, resulting in a combined force along the direction normal to the plane of the WTs. This force is referred to as the aerodynamic thrust and can be presented by Lee et al. [24].

$$F_T = 0.5\rho_a \pi R_T^2 V_s^2 (1 + 2v_s/V_s) C_T \tag{16}$$

where $F_T$ denotes the thrust force; $\rho_a$ denotes the air density; $V_s$ and $v_s$ denote the mean and fluctuating wind velocity, respectively; $R_T$ denotes the rotor radius; $C_T$ denotes the thrust coefficient and can be presented by

$$C_T = 4a_1 - a \tag{17}$$

where $a$ is the induction factor.

The mean wind velocity $V(z)$ can be calculated by [25].

$$V(z) = V_{ref}\left(z/z_{ref}\right)^{\beta} \tag{18}$$

where $z$ and $z_{ref}$ are tower height and wind velocity measuring height, respectively; $V_{ref}$ is wind velocity at $z_{ref}$; and $\beta$ is a terrain roughness parameter.

The fluctuating wind velocity can be described by the cross-power spectral. In this study, the cross-power spectral of Simiu [26] is used.

$$\frac{nS_v(z,n)}{v_*^2} = \frac{200f}{(1+50f)^{5/3}} \tag{19}$$

and $f = nz/V$ is a dimensionless parameter, $n$ is the frequency, $v^*$ is the wind shear velocity and can be calculated by

$$v^* = \frac{k_a}{ln\left(z_{ref}/z_0\right)} V_{10} \tag{20}$$

where $z_0$ is the roughness length and this study uses $z_0 = 0.01$, $k_a = 0.04$ is Von Karman's constant.

Based on the blade element momentum theory and first-order Taylor formula, the aerodynamic forces are expressed as viscous damping force, in which the aerodynamic damping $c_x$ can be calculated by [27]

$$c_x = N_b \int_0^R (A + B) dr \tag{21}$$

$$A = \frac{\partial(p_{\mathrm{N0}})}{\partial V_x} = \frac{\rho_a c(r) V_x}{sin^2\,\varphi} C_n$$
$$B = \frac{\partial(p_{\mathrm{N0}})}{\partial \varphi}\frac{d\varphi}{dV_x} \tag{22}$$

$$C_n = C_L\, cos\,\varphi + C_D\, sin\,\varphi$$
$$C_t = C_L\, sin\,\varphi - C_D\, cos\,\varphi \tag{23}$$

$$V_x = V_W(1 - a) \tag{24}$$

$$p_{\mathrm{N0}} = \frac{1}{2}\rho_a \frac{{V_x}^2}{sin^2\,\varphi} c(r) C_n \tag{25}$$

$$\frac{\partial(p_{\mathrm{N0}})}{\partial\varphi} = \frac{1}{2}\rho {V_x}^2 \frac{\frac{dC_n}{d\varphi} - \frac{2C_n}{tan\varphi}}{sin^2\,\varphi} c(r) \tag{26}$$

$$\frac{dC_n}{d\varphi} = \left(\frac{dC_L}{d\varphi} + C_D\right) cos\,\varphi + \left(\frac{dC_D}{d\varphi} - C_L\right) sin\,\varphi \tag{27}$$

$$\frac{d\varphi}{dV_x} = \frac{1}{\omega_1 r\left(\frac{1+a'}{cos^2\,\varphi} + \frac{da'}{d\varphi} tan\,\varphi\right)} \tag{28}$$

$$\frac{da'}{d\varphi} = -\frac{4\left(2\,cos(2\varphi)\,C_t - \frac{dC_t}{d\varphi} sin\,\varphi\,cos\,\varphi\right)}{\sigma(C_t)^2\left(\frac{4\,sin\,\varphi\,cos\,\varphi}{\sigma C_t} - 1\right)^2} \tag{29}$$

$$tan\,\varphi = \frac{V_x}{\omega_1 r(1+a')} \tag{30}$$

$$a = \frac{1}{\frac{4\,sin^2\,\varphi}{\sigma C_n} + 1} \tag{31}$$

$$a' = \frac{1}{\frac{4\,sin\,\varphi\,cos\,\varphi}{\sigma C_t} - 1} \tag{32}$$

$$\sigma = \frac{c(r) N_b}{2\pi r} \tag{33}$$

where $N_b$ and $R$ are the number and length of blades, respectively; $a$ and $a'$ are the axial and the tangential induction factor, respectively; $C_L$ and $C_D$ are coefficients of lift and drag for the blade, respectively; $V_W$ is the wind speed; $\varphi$ is the angle between the relative velocity and the plane of rotation; $c$ is the chord length of the blade; $\omega_1$ is the rotational speed of the rotor; $r$ is the distance between the blade and the blade root; $p_{\mathrm{N0}}$ refers to the aerodynamic lift of the blade at a specific radius $r$, projected in the direction normal to the rotor plane. This lift is the force generated by the airfoil section of the blade due to aerodynamic forces, and its projection helps in determining the contribution of the lift to the overall performance of the rotor at a given radius; and $\sigma$ represents the fraction of the area within the volume that is occupied by the blades.

### *2.4. Damping Calculating Method*

In wind turbine engineering design, a simplified method is commonly employed that uses a total damping factor to account for the contributions from various sources of damping. This total damping factor is the sum of the individual damping factors from structural, soil, aerodynamic, and other damping sources. The total damping factor for the simplified damping model can be expressed as

$$\xi_{\mathrm{total}} = \xi_{\mathrm{struc}} + \xi_{\mathrm{soil}} + \xi_{\mathrm{aero}} + \xi_{\mathrm{other}} \tag{34}$$

where $\xi_{\mathrm{total}}$, $\xi_{\mathrm{struc}}$, $\xi_{\mathrm{soil}}$, $\xi_{\mathrm{aero}}$ and $\xi_{\mathrm{other}}$ respectively denote the total, structural, soil, aerodynamic damping, and other damping sources, such as hydrodynamic and supplemental damping.

The method of calculating the damping ratio can refer to the study of Jiang et al. [20]. The logarithmic decrement is determined using the following formula:

$$\delta = \frac{1}{n}\ln\left(\frac{A_1}{A_n}\right) \tag{35}$$

$$\xi = \frac{1}{\sqrt{1+(2\pi/\delta)^2}} \tag{36}$$

in which $A_1$ and $A_n$ are two amplitudes $n$ periods apart.

In this study, the process of calculating aerodynamic damping ratio and soil damping ratio is shown in Figure 3. The simulation of soil damping is modeled in the form of soil resistance, as shown in Equation (6). The aerodynamic damping is simulated by a damper at the tower top Wang et al. [28]. Two finite element models are established: with soil resistance but no tower top damper (Figure 3a), and no soil resistance but with tower top damper (Figure 3b). Through the free vibration time history of two models after an impulse excitation and Equations (35) and (36), the precise soil damping ratio and aerodynamic damping ratio can be calculated.

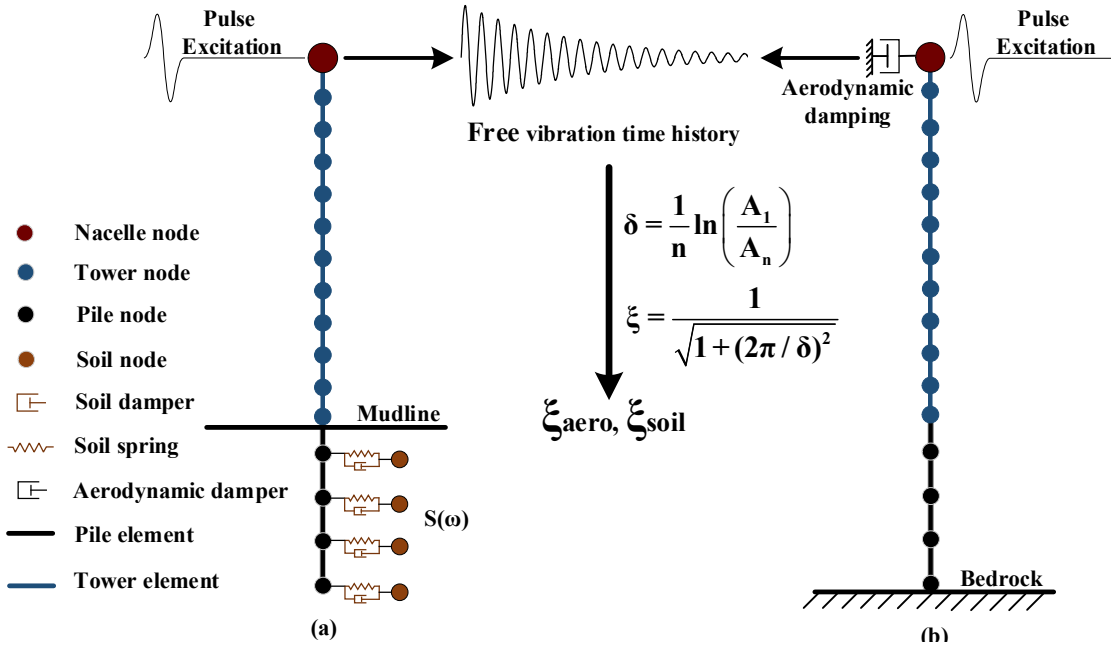


**Figure 3.** The process of calculating the $\xi_{aero}$ and the $\xi_{soil}$. (**a**) Model of soil damping, (**b**) model of aerodynamic damping.

## 3. Results and Discussion

This study utilizes the detailed documents of an OWT from the National Renewable Energy Laboratory published. Table 1 summarizes the main characteristics of the selected turbines.

**Table 1.** 5 MW OWT model properties.

| Property | Value |
|---|---|
| Rotor diameter | 126 m |
| Rotor-Nacelle mass | 350,000 kg |
| Tower height | 87.6 m |
| Base and top diameter | 6 m and 3.97 m |
| Base and top thickness | 0.027 m and 0.019 m |
| Monopile length | 40 m |
| Monopile diameter | 6 m |
| Density of monopile | 7500 kg/m$^3$ |
| Density of tower | 8500 kg/m$^3$ |
| E (Young's modulus) | 210 GPa |
| Poisson ratio | 0.3 |

The length and the diameter of the monopile are 40 m and 6 m, respectively. The tower's bottom diameter is 6 m, tapering to 3.87 m at the top. The tower's wall thickness decreases linearly from 0.027 m to 0.019 m along the tower. The rotor has a diameter of 126 m, and both the monopile and tower are constructed from standard steel. The material

properties can be seen in Table 1. Considering the painting, welds, bolts, and flanges during construction, the material density of the tower is 8500 kg/m$^3$. The damping ratio of the structure and soil are 0.02 and 0.05 in this study, respectively. Figure 4 shows the aerodynamic damping $c_x$ versus the wind velocity $V_s$.

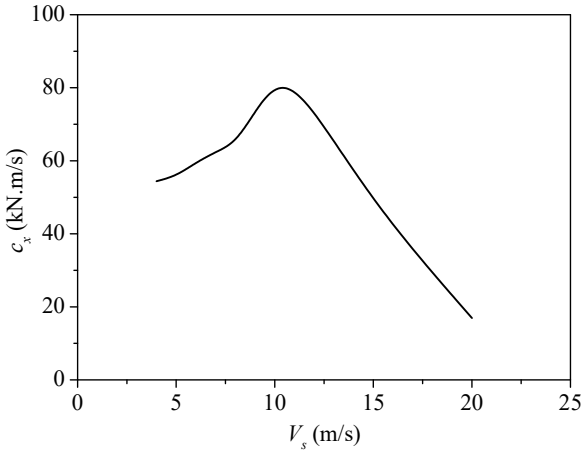


**Figure 4.** The relationship of aerodynamic damping $c_x$ and the wind velocity $V_s$.

To evaluate the influence of soil and aerodynamic damping on the dynamic response of OWT under wind load or seismic load, a dimensionless parameter $R_i$ is defined as

$$R_i = \frac{u_0 - u_a}{u_a} \tag{37}$$

where $u_0$ and $u_a$ are the peak displacement of the OWT at tower top without soil and aerodynamic damping and considering aerodynamic damping and soil, respectively.

To assess the precision of the simplified damping model, the following steps were taken, a dimensionless parameter $R_e$ is defined as

$$R_e = \frac{u_e - u_a}{u_a} \tag{38}$$

where $u_e$ is the peak displacement of the OWT at tower top using the simplified damping model.

### *3.1. Soil Damping*

The damping ratio of soil ($\xi_{\text{soil}}$) for the OWT can be obtained by Equations (35) and (36). Figure 5 shows the correlation between the soil's equivalent damping ratio and its elastic modulus ($E_s$). It is evident that the damping ratio decreases as the soil stiffness increases, and it remains within the range of 0.15% to 0.45% when $E_s$ is greater than or equal to 10 MPa.

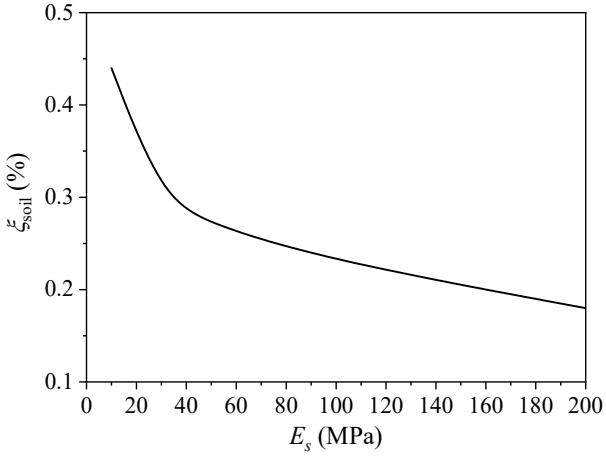


**Figure 5.** Soil damping ratio versus with $E_s$.

Figures 6 and 7 demonstrate the effects of soil damping under thrust force and earthquakes, respectively. As shown in Figure 6, soil damping reduces the dynamic responses of the OWT subjected to operating conditions, with the reduction being less than 6.0% for the monopile foundation, regardless of the soil's elastic modulus. In Figure 7, it is observed that soil damping also mitigates the dynamic responses of the OWT, and this influence decreases gradually with the increasing stiffness of the soil.

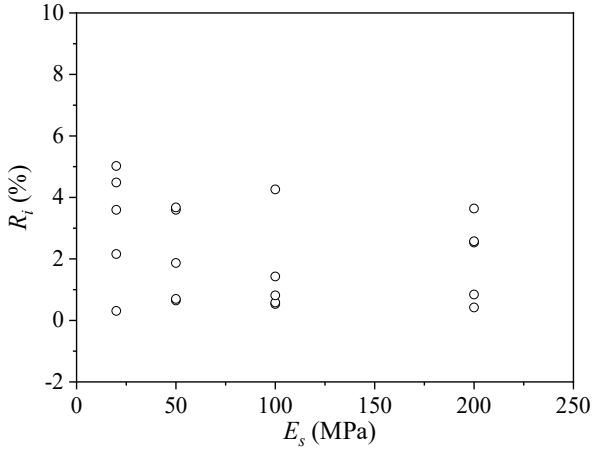


**Figure 6.** Effect of soil damping to OWT under thrust force with $V_s$ = 11.4 m/s.

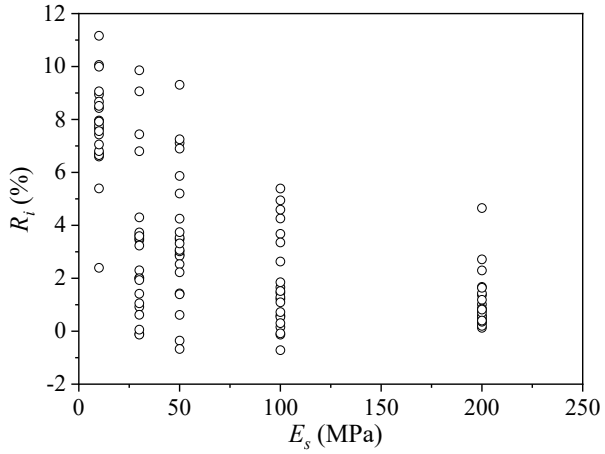


**Figure 7.** Effect of soil damping to OWT under seismic load.

Figures 8 and 9 assess the accuracy of the simplified method for soil damping. Figure 8 evaluates the performance of the simplified soil damping model for the OWT under operating conditions. The results reveal that this model offers high accuracy for the OWT's dynamic responses under thrust force, with an error of less than 2%. Figure 9 demonstrates the precision of the simplified soil damping model for the OWT under seismic load, specifically with an elastic modulus of soil ($E_s$) of 30 MPa. It can be concluded that the simplified damping model of soil may have a big error in calculating the seismic responses of the OWT.

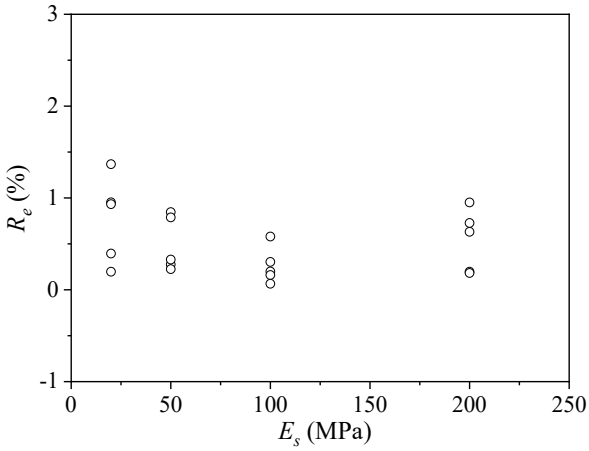


**Figure 8.** The accuracy of the simplified damping model of soil for the OWT under thrust force with $V_s$ = 11.4 m/s.

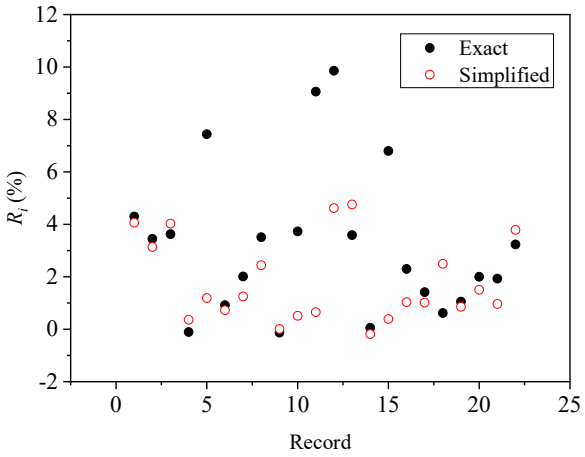


**Figure 9.** The precision of the simplified damping model of soil for the OWT under seismic load with $E_s$ = 30 MPa.

### *3.2. Aerodynamic Damping*

The damping ratio of aerodynamic ($\xi_{aero}$) for the OWT can be obtained by Equations (35) and (36). Figure 10 illustrates the relationship between the aerodynamic damping ratio and the mean wind velocity ($V_s$). It is evident that the aerodynamic damping ratio exhibits a non-monotonic trend, initially increasing and then decreasing as $V_s$ rises, and within a range of 5%.

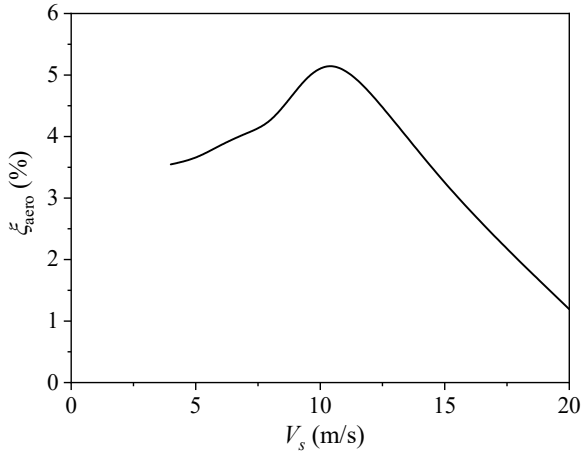


**Figure 10.** Aerodynamic damping ratio versus with $V_s$.

Figures 11 and 12 illustrate the effect of aerodynamic damping on the OWT under thrust force and seismic load, respectively. The results demonstrate that aerodynamic damping effectively minimizes the dynamic responses in both

operating and seismic conditions. In particular, at the rated wind speed, aerodynamic damping can reduce the seismic responses by as much as 65%. This underscores the significance of considering aerodynamic damping in the OWT design.

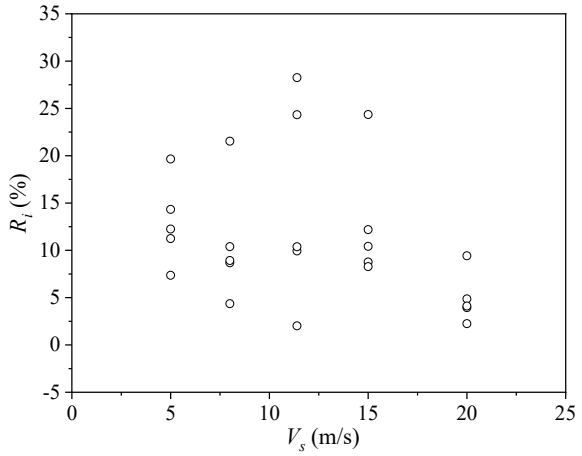


**Figure 11.** Effect of aerodynamic damping to OWT subjected to the thrust force.

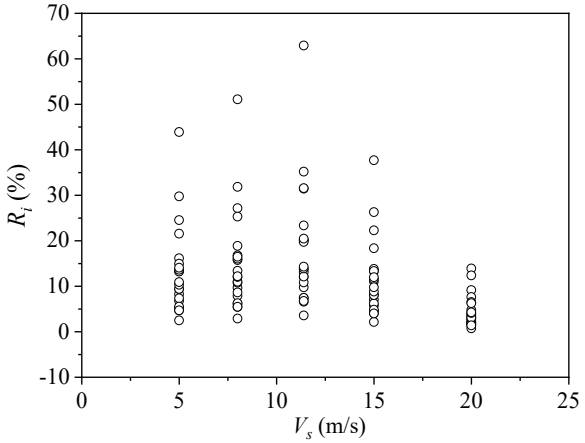


**Figure 12.** Effect of aerodynamic damping to OWT subjected to seismic load.

Figures 13 and 14 show the accuracy of the simplified method for aerodynamic damping. Figure 13 demonstrates the precision of the simplified aerodynamic damping model for the OWT under operating conditions. The results revealed the model accurately analyzes the response of the OWT under thrust force, with an error of less than 2%. Figure 14 shows the precision of the simplified damping model of aerodynamic for the OWT under seismic load with $V_s$ = 11.4 m/s. The results indicate that the simplified damping model of aerodynamic has a great error in calculating the responses of the OWT and the highest error even reaches 60%.

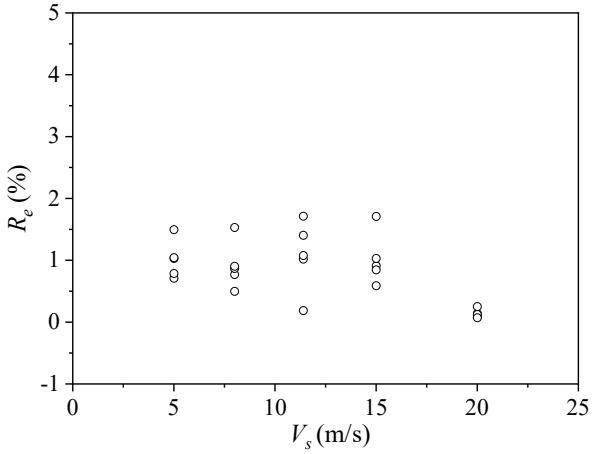


**Figure 13.** The accuracy of the simplified damping model of aerodynamics for the OWT under thrust force.

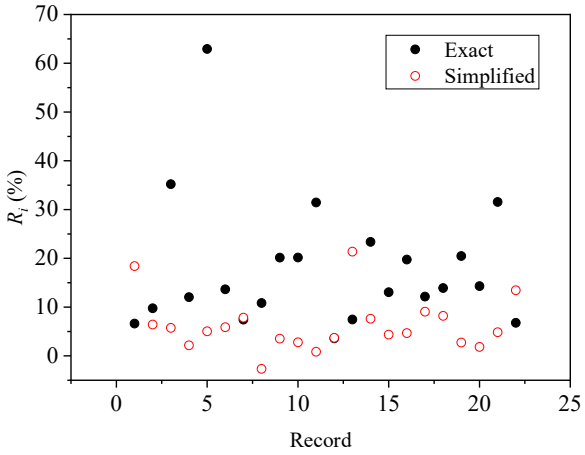


**Figure 14.** The precision of the simplified damping model of aerodynamic for the OWT under seismic load with $V_s$ = 11.4 m/s.

## 4. Conclusions

This study investigates the influences of aerodynamic and soil damping on OWT. It assesses the accuracy of the simplified damping method by analyzing the dynamic response of the 5 MW turbine under seismic and wind load conditions. The main conclusions are as follows:

(1) The equivalent damping ratio of soil decreases with the increasing stiffness of the soil and it is in the range of 0.15–0.45% when the elastic modulus of soil is larger than 10 MPa. The damping ratio of aerodynamics increases firstly and then decreases with the increase of wind speed and it can reach 5% in rated wind speed.

(2) Both soil and aerodynamic damping are crucial in mitigating the dynamic responses of OWT. The impact of soil damping on seismic responses diminishes as soil stiffness increases. Moreover, it is important to note that aerodynamic damping has a much stronger effect on the response of the OWT compared to soil damping.

(3) The simplified damping model of soil and aerodynamics has high precision for evaluating the dynamic responses of OWT under wind load. However, the error is much larger for the seismic responses, especially for the aerodynamic damping. Therefore, it is unreasonable to use the simplified damping model in the seismic design of OWT.

## Acknowledgments

This research is funded by the National Natural Science Foundation of China (52278480). The support is gratefully acknowledged. The results and conclusions presented are of the authors and do not necessarily reflect the view of the sponsors.

## Author Contributions

Conceptualization, P.W. and R.X.; Methodology, P.W. and R.X.; Software, P.W. and Y.B.; Validation, P.W., R.X. and Y.B.; Formal Analysis, Y.B.; Investigation, Y.Q.; Resources, Y.Q.; Data Curation, P.W. and R.X.; Writing—Original Draft Preparation, P.W. and R.X.; Writing—Review & Editing, Y.B., P.W. and R.X.; Visualization, Y.Q.; Supervision, X.D.; Project Administration, X.D.; Funding Acquisition, P.W.

## Ethics Statement

Not applicable.

## Informed Consent Statement

Not applicable.

## Data Availability Statement

Data will be made available on request.

## Funding

This research is funded by the National Natural Science Foundation of China (52278480), and Chongqing Natural Science Foundation (CSTB2024NSCQ-MSX1108).

## Declaration of Competing Interest

The authors declare that they have no known competing financial interests or personal relationships that could have appeared to influence the work reported in this paper.

## References

1. Herzig G. *Global Offshore Wind Report 2020*; World Forum Offshore Wind: Singapore, 2021.
2. Yang J, Liu Q, Li X, Cui X. Overview of wind power in China: Status and future. *Sustainability* **2017**, *9*, 1454.
3. Chen C, Duffour P. Modelling damping sources in monopile-supported offshore wind turbines. *Wind. Energy* **2018**, *21*, 1121–1140.
4. Shirzadeh R, Devriendt C, Bidakhvidi MA, Guillaume P. Experimental and computational damping estimation of an offshore wind turbine on a monopole foundation. *J. Wind. Eng. Ind. Aerod.* **2013**, *120*, 96–106.
5. Cheng Y, Luo Y, Wang J, Dai K, Wang W, Damatty A. Fragility and vulnerability development of offshore wind turbines under aero-hydro loadings. *Eng. Struct.* **2023**, *293*, 116625.
6. Wang P, Bai Y, Wang M, Zhao M, Du X. Seismic Vulnerability and Performance-based Assessment of Monopile Offshore Wind Turbine Considering Turbine Blades. *Soil Dyn. Earthq. Eng.* **2024**, *186*, 108918.
7. Ali A, De Risi R, Sextos A, Goda K, Chang Z. Seismic vulnerability of offshore wind turbines to pulse and non-pulse records. *Earthq. Eng. Struct. Dyn.* **2019**, *49*, 24–50.
8. Valamanesh V, Myers A. Aerodynamic damping and seismic response of horizontal axis wind turbine towers. *J. Struct. Eng.* **2014**, *140*, 11.
9. Feyzollahzadeh M, Mahmoodi MJ, Yadavar-Nikravesh SM, Jamali J. Wind load response of offshore wind turbine towers with fixed monopile platform. *J. Wind Eng. Ind. Aerod.* **2016**, *158*, 122–138.
10. Rendon EA, Manuel L. Long-term loads for a monopile-supported offshore wind turbine. *Wind Energy* **2014**, *17*, 209–223.
11. Garrad AD. Forces and dynamics of horizontal axes wind turbines. In *Wind Energy Conversion Systems*; Prentice Hall: New York, NY, USA, 1990; pp. 119–142.
12. Chen C, Duffour P, Dai K, Wang Y, Fromme P. Identification of aerodynamic damping matrix for operating wind turbines. *Mech. Syst. Signal. Process.* **2021**, *154*, 107568.
13. Carswell W, Johansson J, Løvholt F, Arwade SR. Foundation damping and the dynamics of offshore wind turbine monopiles. *Renew. Energy* **2015**, *80*, 724–736.
14. Van Buren E, Muskulus M. Improving pile foundation models for use in bottom-fixed offshore wind turbine applications. *Energy Procedia* **2012**, *24*, 363–370.
15. Wang P, Zhang W, Xu H, Zhao M, Du X. A high-accuracy substructure method in the time domain for simulating pile-soil dynamic interaction in horizontal vibration. *Comput. Geotech.* **2021**, *140*, 104479.
16. Wang P, Zhao M, Zhang B, Xu H, Du X. Effects of rocking impedance and soil shear stress of the free-field on the dynamic response of an end-bearing pile during horizontal earthquakes. *Comput. Geotech.* **2022**, *150*, 104919.
17. Versteijlen W, Metrikine A, Hoving J, Smid E, de Vries W. Estimation of the vibration decrement of an offshore wind turbine support structure caused by its interaction with soil. In Proceedings of the EWEA Offshore 2011 conference, Amsterdam, The Netherlands, 29 November–1 December 2011.
18. Tarp-Johansen NJ, Andersen L, Christensen E, Mørch C, Kallesøe B, Frandsen S. Comparing sources of damping of cross-wind motion. In Proceedings of the European Offshore Wind 2009, Stockholm, Sweden, 14–16 September 2009.
19. Damgaard M, Andersen J, LB I, Andersen L. Time-varying dynamic properties of offshore wind turbines evaluated by modal testing. In Proceedings of the 18th International Conference on Soil Mechanics and Geotechnical Engineering, Paris, France, 2–6 September 2013; pp. 2343–2346.
20. Jiang J, Lian J, Dong X, Wang H, Zhou H. Soil damping calculation of the offshore wind turbine supported by wide-shallow bucket foundation. *Appl. Ocean Res.* **2021**, *111*, 102682.
21. Huang Y, Wang P, Zhao M, Zhang C, Du X. Dynamic responses of an end-bearing pile subjected to horizontal earthquakes considering water-pile-soil interactions. *Ocean Eng.* **2021**, *238*, 109726.
22. Applied Technology Council. *Quantification of Building Seismic Performance Factors: Component Equivalency Methodology (FEMA P695)*; FEMA: Washington, DC, USA, 2009.
23. Wang P, Zhao M, Du X, Liu J, Xu C. Wind, wave and earthquake responses of offshore wind turbine on monopile foundation in clay. *Soil Dyn. Earthq. Eng.* **2018**, *113*, 47–57.

24. Lee S, Kim H, Lee S. Analysis of aerodynamic characteristics on a counter-rotating wind turbine. *Curr. Appl. Phys.* **2010**, *10*, 339–342.
25. DNV. *Environmental Conditions and Environmental Loads (DNV-RP-C205)*; Det Norske Veritas: Oslo, Norway, 2010.
26. Simiu E. Wind spectra and dynamic along wind response. *J. Struct. Div.* **1974**, *100*, 1897–1910.
27. Xi R, Wang P, Du X, Xu K, Xu C, Jia J. A semi-analytical model of aerodynamic damping for horizontal axis wind turbines and its applications. *Ocean Eng.* **2020**, *214*, 107861.
28. Wang M, Bai Y, Wang P, Zhao M, Du X. Cloud-based seismic fragility analysis of operating offshore wind turbine with stochastic coupling of wind-wave-earthquake excitations. *Thin-Wall. Struct.* **2025**, *208*, 112858.